Studies of the m/n=2/1 Neoclassical Tearing Mode Onset and Structure in the National Spherical Torus Experiment

S.P. Gerhardt[1], R. J. La Haye[2], R. Buttery[3], D.P. Brennan[4], E. Strait[2], S. Sabbagh[5], M. Bell[1], R. Bell[1], E. Fredrickson[1], D. Gates[1], B. LeBlanc[1], J. Menard[1], D. Stutman[6], K. Tritz[6], H. Yuh[7]

[1] Princeton Plasma Physics Laboratory
[2] General Atomics
[3] EURATOM/UKAEA Fusion Association, Culham Science Centre, Abingdon, Oxon, OX14 3DB, United Kingdom
[4] University of Tulsa
[5] Columbia University
[6] The Johns Hopkins University
[7] Nova Photonics

Abstract

The m/n=2/1 neoclassical tearing mode onset and mode structure studies in the National Spherical Torus Experiment [M. Ono, et al., Nuclear Fusion **40**, 557 (2000)] are described. At least three different mechanisms can trigger the mode: energetic particle modes (EPM), edge localized modes (ELMs), and "triggerless" cases, where the mode appears to grow from small amplitude without a seeding perturbation. In all cases, the 2/1 mode is coupled to a 1/1 mode, increasing the performance degradation beyond that expected for a large single-helicity island. Little or no correlation is found between the required drive at onset and the plasma rotation, either in absolute terms or in the E_R=0 rotation frame. However, for each triggering type, the required drive increases when the flow shear at the q=2 surface is increased. For fixed rotation shear, the required NTM drive at onset (at the q=2 surface) is smallest with EPM triggered cases and largest in the trigger-free cases, with the ELM triggered cases triggering at intermediate values. A comparison is made to published theories regarding the affect of flow shear on tearing modes.

Outline:

1: Introduction
2: Formulation of NTM Problem
3: Diagnostics and Discharges Utilized in This Study
4: Examples of Triggers
5: Studies of the Mode Eigenfunction Using Ultra-Soft X-rays
6: Onset Thresholds vs Rotation and Trigger Type
7: Discussion
8: Conclusions
9: Acknowledgements
Appendix: Comparison of the various bootstrap current definitions.
References

1: Introduction

The neoclassical tearing mode [Chang 1995, Gates 1997, LaHaye 1997, Zohm 1997, Sauter 1997, Huysmans 1999] is a prominent β-limiting instability in any positive-shear tokamak plasma. The driving agent for this mode is the pressure flattening inside a magnetic island due to rapid parallel transport, which leads to a local loss of the pressure driven bootstrap current [Peters 2000]. This loss of current acts like a helically perturbed current in the direction opposite the bootstrap current, and drives a "neoclassical" magnetic island. This island can lead to large confinement degradations [Chang 1990], rotation damping due to interaction with the resistive wall and error fields [Fitzpatrick 1993], and sometimes disruptive termination of the plasma pulse. Furthermore, these modes have been observed in spherical torus (ST) plasmas [Peng 1986], despite enhanced pressure-curvature effects at low aspect ratio [Kruger 1998, Hegna 1998]. A comprehensive recent review is given in [La Haye 2006].

Much progress has been made in understanding and controlling these modes (see Ref. [La Haye 2006]) for a recent review), but many outstanding issues remain. One important issue is with regard to plasma rotation: most studies of NTMs have been made in plasmas with dominant co-injection providing rapid plasma rotation, while future burning plasmas, whether at conventional aspect ratio like ITER [Shimada 2007] or an ST [Najmabadi 2003], will not have this torque source. Hence, assessing NTM physics at low-rotation (or rotation shear) is important when assessing the stability of these next-step devices. Furthermore, this paper demonstrates that even rapidly rotating ST plasmas must contend with these instabilities, a result of importance for ST component test facility (CTF) [Peng 2005, Peng 2008] designs.

A second issue comes up with regard to the NTM triggering mechanism, as the NTM is often considered to be metastable (i.e. "small" perturbations decay, while "large" ones grow, where "small" and "large" are determined by the mode physics [La Haye 2006]). In order to avoid NTMs, it is often thought wise to operate conventional aspect ratio tokamaks with either a rapid sawtooth cycle [Sauter 2002], or in a "hybrid" configuration [Luce 2001, Sips 2002, Joffrin 2003, Wade 2005, Brennan 2005, La Haye 2008] with $q_{min}\geq 1$ and no sawtooth triggers. However, many modes other than sawteeth can destabilize an NTM, and it is important to assess the trigger types available in different plasma regimes, including $q_{min}>1$ cases.

In order to address the issue of rotation and the m/n=2/1 NTM (here, m is the poloidal mode number and n the toroidal mode number), a devoted experiment was carried out in DIII-D [Buttery 2008]. These experiments utilized that devices unique ability to control the plasma rotation through a mixture of co- and counter- injected neutral beams. It was shown that the value of β_N ($\beta_N=\beta a B_T/I_P$) at mode onset was reduced as the net co-directed torque was reduced to zero. An analysis of various NTM physics mechanisms lead to the hypothesis that it was actually rotation shear, not rotation, that modified the threshold. However, in those discharges, rotation and rotation shear increased or

decrease together, so it was impossible to prove that shear was the dominant effect.

The above discharges were designed to always have a 3/2 NTM proceed the 2/1 onset, allowing an opportunity to study the impact of flow or flow shear on the saturated 3/2 island [La Haye 2009]. It was found that the width of the 3/2 island increased as the toroidal flow-shear was reduced. This result was explained by the viscous distortion of the island leading to a stabilizing coupling of magnetic shear to rotation shear. The measured island widths and pressure gradients were used to determine the classical tearing stability index $\Delta'r$ as a function of flow shear as

$$\Delta' r = C_1 + C_2\left(\frac{d\omega}{dR} L_s \tau_A\right), \qquad \text{(X)}$$

where $L_s = qL_q/\varepsilon$, $\tau_A = R_0(\mu_o m_i n_i)^{1/2}/B_{T0}$, and $d\Omega/dR$ is the outboard midplane angular rotation frequency derivative in rad/sec/m.

A similar m/n=2/1 mode experiment was run in the National Spherical Torus Experiment [Ono 2000]: n=3 non-resonant braking [Zhu 2006] was used to reduce the plasma rotation, and the β_N value at mode onset was recorded as a function of the rotation frequency at q=2 for two different values of the elongation κ. A reduction in the onset β_N was indeed found with reduced rotation. However, there was a strong correlation between flow and flow shear for this small dataset, making it difficult to determined which parameter was more important. A search was then made for similar discharges with 2/1 modes, allowing an expanded database. However, the apparent scatter in the data began to increase as more discharges were added. After detailed analysis, it became clear that a number of factors were contributing to the scatter: i) the mechanism by which the mode is triggered influences the onset threshold, ii) the more relevant drive parameter for an NTM in NSTX is the bootstrap drive at the rational surface, not the global normalized-β, and iii) flow shear is a better parameter than flow for determining the onset. It is the purpose of this paper to summarize these results.

It is found that at least three types of mode-onset occur: NTMs triggered by energetic particle modes (EPMs), triggered by edge localized modes (ELMs), or growing after no discernable trigger. The NTM drive at onset is lowest for the EPM cases, and highest for the “triggerless” cases, with the ELM cases triggering at intermediate drive. Within each trigger type or for the data set as a whole, there is a better correlation of the onset drive with rotation shear than with rotation. A comparison with the published literature on NTMs and tearing modes (TMs) and rotation does not yield a clear explanation of the results, although some models do predict increased stability with increasing flow shear. These results offer the first ever discussion of NTM triggers in a $q_{min}>1$ ST plasma, and provide the strongest evidence yet that rotation shear, and not simple rotation, plays an important role in setting the NTM onset threshold.

Additionally, the fluctuating ultra-soft X-ray emission was utilized to constrain models for the mode eigenfunction. While a simple m/n=2/1 island model can reproduce the emission fluctuations for chords in the vicinity of the q=2 surface, there is significant disagreement between the measurements and modeling for the core chords. This problem is resolved by adding an m/n=1/1

kink eigenfunction to the island model. The consequences of this coupled mode are briefly discussed.

The organization of this paper is a follows. Sect. 2 provides the formulation of the NTM physics utilized in this manuscript, while Sect. 3 provides some technical details about the experiments. Sect. 4 illustrates the three trigger varieties for the 2/1 mode in NSTX, and briefly indicates the effect of the mode on plasma performance. A study of the mode eigenfunction is provided in Sect. 5. Sect. 6 presents the main result: the dependence of the onset NTM drive on trigger type and rotation shear. A comparison to published simulation results regarding rotation shear is provided in Sect. 7, and a summary concludes the paper in Sect. 8.

Note that these results appeared in abbreviated form in [Gerhardt 2009]. The present paper greatly expands on the analysis presented there, while presenting additional new information.

2: Formulation of NTM Problem

A key focus of the present manuscript is in understanding how flow or flow shear impact NTM onset. In order to assess this physics, it is useful to start with the Modified Rutherford Equation [Rutherford 1978], written as:

$$\frac{\tau_R}{r_s^2}\frac{dw}{dt} = \Delta' + \frac{C_{BS}\mu_0 L_q}{B_\theta}\delta j_{BS}\left(\frac{w}{w^2+w_d^2} - \frac{w w_{pol}^2}{w^4+w_b^4}\right) - \frac{6D_R w}{w^2+w_d^2} \qquad \text{(X)}$$

Here, w is the island width, r_s is the minor radius of the resonant surface, and τ_R is the resistive time.

The first term on the RHS represents the classical tearing stability of the current profile [Furth 1963, Furth 1973]. Much theoretical and modeling work [Einaudi 1986, Einaudi 1989, Chen 1990 A, Chen 1990 B, Ofman 1993]. Chandra 2005, Sen 2005, Chandra 2007, Coelho 2007] has indicated that plasma flow can affect the classical tearing stability, a point to be discussed in greater detail in Sect. 7 below.

The second term represents the drive due to the lost bootstrap current (δj_{BS}) inside the magnetic island. For the analysis described here, the missing bootstrap current is calculated from the formulas in Ref. [Sauter 1999] as

$$\delta j_{BS,\,Sauter} = \frac{I(\psi)\,p_e\left(L_{31}\frac{1}{p_e}\frac{dp_e}{d\psi} + L_{32}\frac{1}{T_e}\frac{dT_e}{d\psi}\right)}{\sqrt{\langle B^2\rangle}}\ , \qquad \text{(Xa)}$$

where the terms $I(\psi)$, L_{31}, and L_{32} are defined in that reference. However, as indicated in appendix A1, the approximation

$$\delta j_{OMP} = -\sqrt{\varepsilon}\,\frac{L_q}{L_{Pe}}\beta_{Pe}, \qquad \text{(Xb)}$$

with all terms evaluated at the outboard midplane, is a reasonable approximation to the full calculation, even at low aspect-ratio. The third term on the RHS includes stabilizing effect due to toroidal geometry [Glasser 1975, Hegna 2008], which can also be enhanced by flow or flow shear [Chandra 2005].

The terms w_d, w_{pol}, and w_b describe stabilizing effects relevant to small islands. w_b is the ion banana width $\varepsilon^{1/2}\rho_{\theta I}$, and signifies the stabilizing effect that the bootstrap current is not flattened when the island size is comparable to the ion banana width [Poli 2002]. w_d describes the incomplete flattening of the pressure inside a small magnetic island due to finite perpendicular transport [Fitzpatrick 1995].

The term w_{pol} is a characteristic size for the polarization current effect [Wilson, 1996] and is given by:

$$w_{pol}^2 \propto \left(\frac{L_q}{L_P}\right)^2 g(\varepsilon,\upsilon)\rho_{i,\theta}^2 \frac{\Omega\left(\Omega-\omega_i^*\right)}{\omega_e^{*2}} \qquad \text{(X)}$$

where "g" is a function of collisionality given by g=1 for $\nu<<1$ and $g=e^{-3/2}$ for $\nu>>1$ with $\nu=\nu_i/\varepsilon\omega_e^*$, $\omega_{i,e}^*$ are the electron diamagnetic drift frequencies, and Ω is the frequency of the mode in the $E_R=0$ frame ($\Omega=\omega_{Mirnov}-\omega_{E_R=0}$). The most interesting feature of this term is the clear rotation dependence: the polarization term is predicted to be stabilizing for $0<\Omega<\omega_i^*$, but destabilizing in the regime $\Omega<0$. This term will be discussed in more detail in Sect. 6 as a possible source of the observed rotation dependence of the NTM drive at mode onset.

These small island terms have a stabilizing effect on small islands, i.e. they force dw/dt<0 for islands below a certain width, even in the presence of a large bootstrap drive. Hence, the neoclassical tearing mode is often said to be metastable in that sufficiently small islands do not grow; the islands width must exceed a critical value for the island to grow. However, following Ref. [Brennan 2005] and the observations of "spontaneous" NTMs [Gude 1999, Fredrickson 2002, Brennan 2003], we take the definition that any large magnetic island in a high-β tokamak will have a neoclassical drive, and thus is an NTM.

This discussion of triggers suggests another mechanism, not explicitly included in the MRE, by which rotation could impact the stability of NTMs: differential rotation between the NTM rational surface and the triggering instability surface could reduce the size of the seed islands [Hegna 1999], preventing them from exceeding the metastable threshold. This effect has been used to explain the reduced β_N threshold for the 3/2 NTM is JET when neutral beam injection, which injects both energy and momentum, was replaced by ICRH, which only adds energy [Buttery 2001].

In addition to the definitions of the terms in the MRE, it is important for this study to define with appropriate metrics for the flow shear. The flow shear here is defined as [Buttery 2008, La Haye 2009] $2\pi L_s\tau_A(dF_T/dr)$, where as above $L_s=qL_q/\varepsilon$, $\tau_A=R_0(\mu_o m_i n_i)^{1/2}/B_{T0}$, and the derivative with respect to minor radius is defined as

$$\frac{d}{dr}=\frac{1}{a}\frac{d}{d\rho}, \quad \rho=\sqrt{\frac{\psi-\psi_{edge}}{\psi_{axis}-\psi_{edge}}},$$

where ψ is the poloidal flux and a is the minor radius defined as half the distance between the inboard and outboard separatrix points on the midplane.

One consequence of the MRE is that for large saturated islands, the island width is expected to be proportional to β_P [take (1), use the bootstrap drive from

(2b), and ignore the small island and D_R terms)]. That this is measured to be so is shown in Fig 2. The square-root of the fluctuating poloidal field at the wall, proportional to the magnetic island width [La Haye 2000], is shown as a function of the global β_P, as computed from the EFIT equilibrium code. The observed linear dependence is exactly that expected from a neoclassical island. The MRE also predicts that for small enough islands, the island width will decouple from β_P and go rapidly to zero. This behavior has also been observed in NSTX, and will be reported in a future publication.

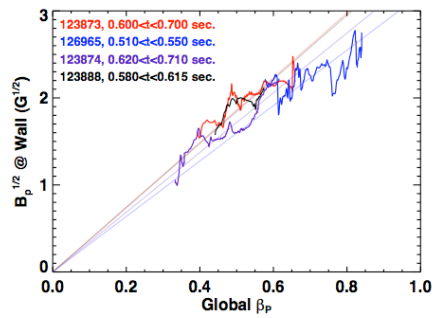

Fig 1. Dependence of the island width $\left(w \propto \sqrt{\tilde{B}_P}\right)$ *on the global poloidal beta.*

3: Diagnostics and Discharges Utilized in This Study

The research presented in this manuscript attempts to utilize the complete NSTX diagnostic set to generate a complete picture of the NTM onset. The mode time evolution is generally studied with a toroidal array of 12 B_p detectors, digitizing the raw sensor voltage at 4 MHz. The signals from multiple sensors are typically decomposed into the various toroidal mode numbers as a function of time, and confirm the n=1 toroidal structure of the mode under study here.

While the analysis of edge magnetic fluctuations can provide much useful information about mode dynamics, the actual mode structure cannot be resolved. For this reason, internal measurements of the island structure are of great interest. Many past studies of NTMs have utilized electron cyclotron emission (ECE) diagnostics to study the temperature perturbation associated with the island [Ren 1998, Meskat 2001, Fredrickson 2003, Hender 2005]. Indeed, the details of the island separatrix shape have even been used to ascertain the value of the classical tearing index Δ' [Ren 1998, Meskat 2001]. However, ECE measurements are not possible in the overdense ST plasmas. Instead, we rely here on measurement of the chord-integrated ultra-soft X-ray (USXR) emission [Stutman 1999]. The present USXR measurement system on NSTX includes two 15-chord diode arrays, each with selectable 100μm, 10μm, 5μm beryllium filters (there is also the option to operate the system in bolometry mode without filters). Further details on the use of this system for mode-structure studies are given in Sect. 5.

With regard to equilibrium profile measurements, the C VI toroidal rotation, ion temperature, and deuteron and CVI density are measured with 10 msec time-resolution at 51 points across the outboard side of the plasma. The electron

density and temperature are measured with a 30 point Thomson Scattering system [Le Blanc 2003], with time resolution of typically 8 msec. The magnetic field pitch angle is measured via the motional Stark effect (MSE) at 12 points on the midplane with 10 msec time resolution. These MSE measurements, coupled to external magnetics and the requirement that the electron temperature be a constant on a magnetic surface, are utilized to constrain the Grad-Schafranov equilibrium by the LRDFIT code.

All data presented in this paper come from discharges similar to the high-κ, high-δ equilibrium illustrated in Fig. 2, which is used for the morning reference shot and for many different experiments. As noted in the introduction, some of the data originated from a devoted experiment to study the dependence of the NTM onset on rotation or rotation shear. With this data as a foundation, similar discharges were found, for a total of 49 in the present database. The parameter ranges present in these discharges are indicated in Table #2. Approximately 1/3 of these discharges use n=3 braking to slow the rotation. Here, ρ_i^* and $\nu_i^*=\nu_i/\varepsilon\omega_{bi}$ are calculated as in Ref [Hender 2004], where, for consistency with previous work, the quantities are evaluated at the outboard midplane:

$$\nu_i^* = \frac{520 n_e \left(10^{19} m^{-3}\right) R q}{\varepsilon^{3/2} T_i^2 \left(eV\right)} \qquad \text{(X)}$$

$$\rho_{\theta,i}^* = \frac{2\times 10^{-4}\sqrt{T_i(eV)}}{r_s B_\theta} \qquad \text{(X)}$$

The range of those two variables in the database is deliberately restricted, although the shape variation may be larger than is typical in an NTM study. This is a consequence of selecting discharges from a wide variety of experiments. However, since NTM stability is anticipated to be largely a local phenomenon, it is anticipated that this will not pose a problem.

Quantity	Units	Minimum Value	Maximum Value
Plasma Current (I_P)	kA	900	1000
Internal Inductance (l_i)	None	0.57	0.8
Elongation (κ)	None	2.05	2.5
Lower Triangularity (δ_l)	None	0.5	0.83
Toroidal Field (B_T)	T	0.43	0.46
q_{95}	None	6.5	9
Injected Power	MW	4	6
β_T	%	11	19
β_N	%·mT/MA	3.25	5.0
ν_i^*	None	0.05	0.11
$\rho_{\theta,i}^*$	None	0.05	0.09

Table #1: Range of parameters allowed in the present database. The quantities are taken at the time of the 2/1 mode onset.

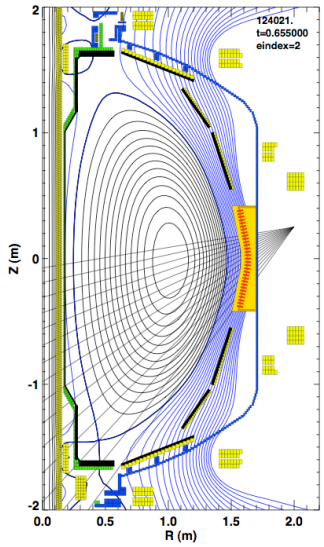

Fig 2. Example high-κ, high-δ equilibrium utilized for this research. Also shows are the USXR chords utilized in for the study of the island eigenfunction.

An example set of profiles included in the database is demonstrated in Fig. 4, where data for three discharges at mode turn-on is shown. The rotation profiles in Fig. 4a) are dramatically different, owing to the use of different n=3 braking levels in the red and green cases. The electron pressure profiles in 4c) virtually overlay, and the ion temperatures in the vicinity of q=2 ($R_{q=2}$~1.35m) are very similar (Fig. 4d). There are subtle differences in the reconstructed q profiles in Fig 4b) that will lead to variation in the NTM drive. However, this is accounted for in the formulation presented above and does not impede the analysis of flow or flow shear effects.

With these profiles in mind, figure 5 shows the range of rotation and rotation velocity achieved in the database. There is some co-linearity in the data set, especially for the ELM triggered modes represented with blue points, and care must be taken in attempting to separate the effects of flow and flow shear on the NTM onset. This will be done in Sect. 6 using simple statistical arguments. For the EPM and “triggerless modes”, there is reasonable separation between these two variables.

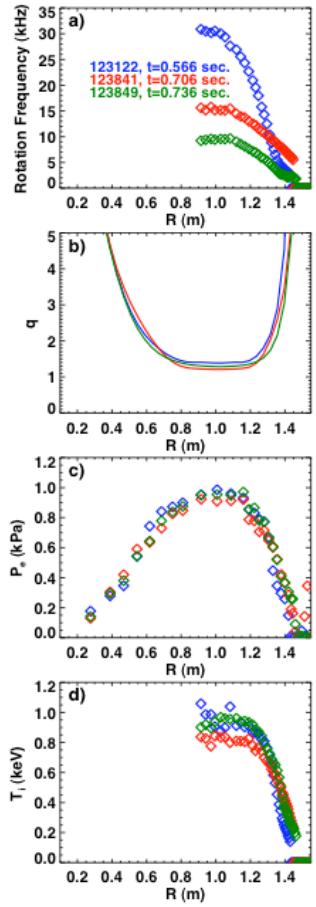

Fig 3. Example profiles at the time of mode onset. Shown are the a) rotation frequency, b) safety factor, c) electron pressure, and d) ion temperature.

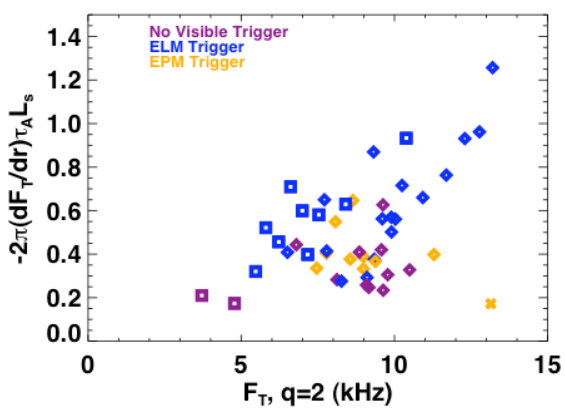

Fig 4. Rotation at q=2 vs rotation shear at q=2, for all discharges in the present database. The color scheme is explained in Sect. 6.

4: Examples of Triggers

In this section, the early time evolution of three example m/n=2/1 modes is shown. All of the modes in these three examples, and this paper generally, have a number of distinguishing characteristics. They are of course n=1 modes, as determined from the mode phase measured by a toroidal array of Mirnov coils. The mode frequency at onset is either very near to or quickly approaches the rotation frequency of the q=2 surface, and the frequency of the saturated mode is always tied to the q=2 rotation frequency. Furthermore, the rotation evolution just after the mode strikes typically shows a flat spot near q=2. Flat spots are observed in the electron temperature profile at q=2 (for at least some time-slices, depending on the phase of the O-point with respect to the Thomson scattering laser pulse timing). Each of these points will be elucidated further below and in the following section, in the context of discussing three discharges

A common mechanism by which these NTMs are triggered in NSTX involves seed island formation by energetic particle modes, as illustrated in Fig. 6. A series of chirping modes are observed starting at t=0.55, and continuing until mode onset at 0.605. These modes are visible in the spectrogram in frame a) as near vertical stripes with multiple simultaneous n-numbers, and result in substantial drops in the D-D neutron emission (indicative of the loss of fast particles.) The two n=1 bursts near t=0.55 in particular result in large drops in the neutron rate and plasma rotation. However, it is the large chirping mode at 0.605 that finally results in the mode striking; the chirping behavior is then eliminated for the remainder of the discharge. Note that the rotation in Fig 5e) is observed to drop quickly once the mode strikes, with the rotation inside the q=2 surface falling first. In the final state, the rotation profile is uniform and slow, and is extremely prone to locking followed by disruption.

This example is typical of the EPM triggered modes, in that the final onset of n=1 fluctuations slightly proceeds the drop in the neutron emissions, and the mode frequency at onset is close to the reconstructed q=2 frequency; indeed, these are the two characteristics which will be used to define this trigger type. However, not all cases with an EPM trigger show the island striking at near saturated width as in this example.

Examination of the core USXR data during these triggering EPM modes indicates that they are typically core localized modes, with the USXR signatures localized to r/a<~0.4. They sometimes show a clear phase inversion across the magnetic axis, as would be expected for modes with a strong 1/1 component; other examples show more detailed structures. One can hypothesize that the toroidal coupling of the core 1/1 component to the 2/1 surface produces the observed seed island. Further studies are required in order to verify this hypothesis.

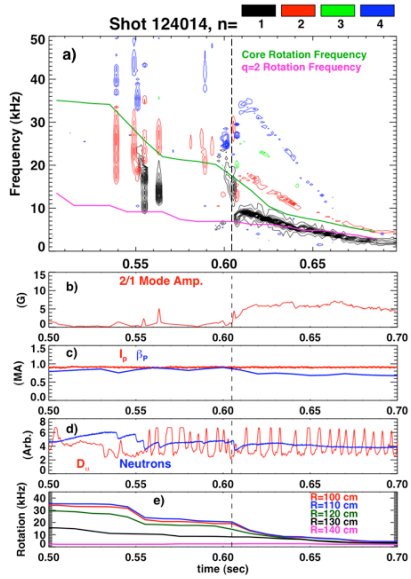

Fig 5. Example case with EPM trigger. Shown are a) the spectrogram of a single Mirnov coil, b) the mode amplitude, c) l_i, the global β_P and I_P, d) the waveforms of both the D_α and neutron emission.

Another common onset mechanism involves triggering by an ELM. These repetitive instabilities are common in many, but not all, high-κ, high-δ discharges in NSTX. While the causes for ELMs are beyond the scope of the present research, the consequences of ELMs in terms of NTM triggering are quite relevant.

An example ELM triggered NTM is shown in Fig. 6. The top frame shows the spectrogram from a single Mirnov coil; the mode is seen to grow from low frequency and low amplitude at t=0.545. Note the series of low-frequency bursts in the spectrogram; these are coincident with the ELMs visible in the D_α frame in frame d) and the edge USXR signal in frame e). The neutron rate and core USXR chord show no perturbation at the time of mode onset, indicating a lack of perturbation in the plasma center. Hence, we conclude that the trigger in this case is apparently the ELM at 0.546. A key observation is that the early mode frequency, i.e. just after it strikes, is dramatically slower than the rotation frequency of the q=2 surface (indicated by the yellow line in the spectrogram). The mode then spins up, reaching the q=2 surface frequency in about 10 msec. The onset of the mode coincident with an ELM, and slow initial frequency followed by dramatic spin-up, are the key signatures of this trigger type.

The evolution of the rotation profile for this case is shown in Fig. 7, where the vertical bar shows the reconstructed location of the q=2 surface for those time slices. Although the mode first shows in the Mirnov spectrogram at t=0.545, the first response in the rotation profile is seen 10 msec later, where a small flat region at q=2 develops. This flat region then expands, with the core rotation dropping and the edge rotation increasing. The final state of this process is a rotation profile which is flat inside of q=2. As noted above, this process of rotation decay appears in every case discussed in this paper. However, the flattening at

q=2 and increase in edge rotation is typically most prominent for those cases that are ELM triggered. This damping will be discussed again in Sect. 5.

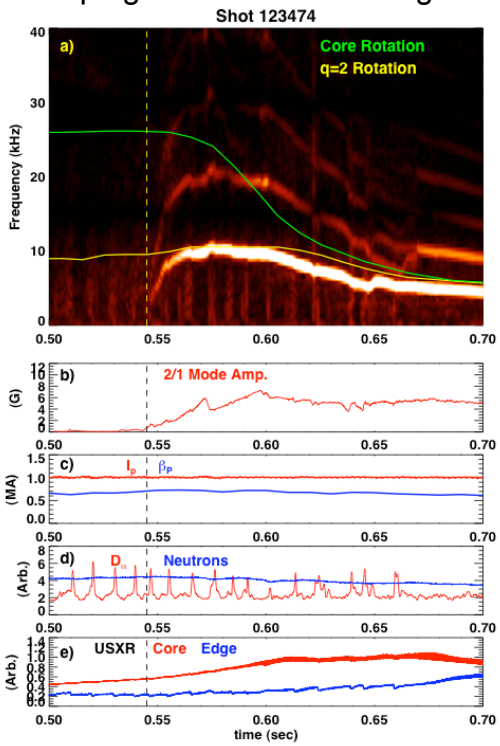

Fig 6. Example case with ELM trigger. Shown are a) the spectrogram of a single Mirnov sensor, b) the mode amplitude, c) the plasma current and global β_P, d) the D-D neutron emission and the divertor D_α emission, and e) core and edge chords from the USXR diagnostic.

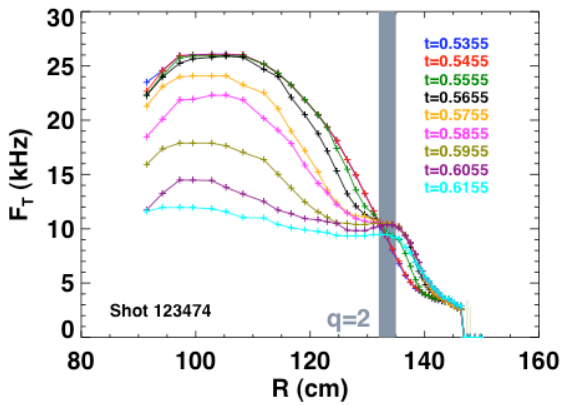

Fig 7. Rotation profile evolution for the shot in Fig. 6, as well as the predicted location of the q=2 surface for the selected time slices.

.

For both the ELM and EPM triggers, the exact nature of the triggering mechanism remains obscure. It seems that the ELM case may be an example of "mixed seeding", as discussed in Ref. [Brennan 2005], where the initial island growth is classical ($\Delta'>0$), but the initial island is due to reconnection driven by

another instability [Brennan 2003]. In the same language, the EPM case may then be an example of “forced seeding.” Proving these hypotheses to be true will require accurate calculations of tearing stability, a challenging proposition [Brennan, 2002] that is only beginning for NSTX

.

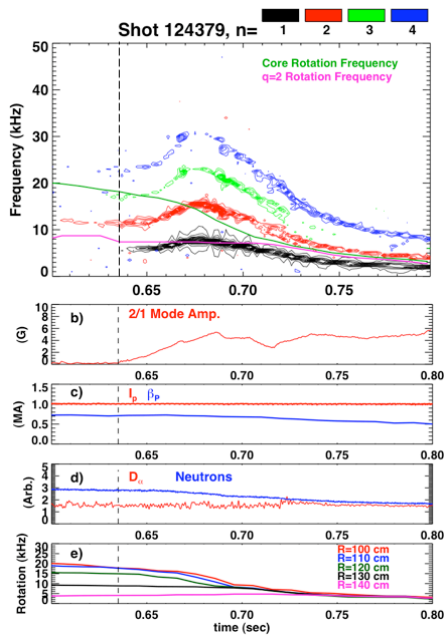

Fig 8. Example case with no apparent trigger. The quantities plotted are the same as in Fig. 6.

Finally, it is not uncommon to see these modes grow with no apparent seeding instability. An example of this behavior is shown in Fig. 8, where the 2/1 mode begins to grow at about t=0.63. The key observation is that there are no perturbations visible on the neutrons emission or the divertor D_α. The mode frequency at onset is very close to that of the q=2 surface, which it subsequently tracks as the rotation decays. Further analysis of this discharge will be presented in the next section.

Note that apparently “seedless” NTMs have been observed in many other devices, including ASDEX-Upgrade [Gude 1999], TFTR [Fredrickson 2002], DIII-D [Buttery 2008, Brennan 2003], and TCV [Reimerdes 2002]. Many explanations have been forthcoming, including the hypotheses that the modes are initially ideally unstable [Fredrickson 2002], that microturbulence provides a stochastic trigger [Itoh 2003, Itoh 2004], that the triggers are present but of undetectably small amplitude in high-β plasmas with low critical island widths [Gude 1999], or that they modes are Δ’ unstable at onset [Reimerdes 2002, Brennan 2003, Brennan 2005]. While the last explanation appears to be a likely candidate for the NSTX cases described here, confirmation will again require the same accurate Δ’ calculations as for the nominally triggered cases.

5: Studies of the Mode Eigenfunction Using Ultra-Soft X-rays

As noted in the introduction, the signals from the edge-magnetics contain limited information on the structure of the mode. For the discharges described in this manuscript, the sole window into the internal structure of the modes come from ultra-soft X-ray emission; this section describes the insights acquired in that way. Given the limited number of chords, tomographic reconstruction of the mode structure, as demonstrated in, for instance, Ref. [Huysmans 1999] is not possible. Instead, the measured USXR emission is utilized to constrain model eigenfunctions.

The procedure utilized here for using USXR emission to study the island structure is as follows. First, the equilibrium helical flux, $\psi_{h,0}(\psi) = \int q(\psi') - q_s d\psi'$, is calculated from the MSE constrained equilibrium. It is then assumed that the USXR emissivity ε is a function of helical flux of $\psi_{h,0}$ alone: $\varepsilon=\varepsilon(\psi_{h,0})$. The equilibria is divided into between 20 and 30 concentric shells equally spaced in physical space, and a matrix $L_{i,j}$ is computed, containing the distance that the ith chord is between the shells j and j+1. The emissivity of the shells can then be calculated from the equation $L\varepsilon=M$, where M is a vector containing the measured emission along the various chords after averaging over many periods of the emission oscillation. Directly inverting this matrix equation to solve for $\varepsilon(\psi_{h,0})$, however, can lead to large emissivity oscillations between adjacent shells as well as negative values of emissivity. In order to avoid this, the "Phillips-Twomey" regularization method [Press, 1992] is used when doing this inversion. The regularization parameters are typically adjusted by hand to achieve a good fit to the measured chordal emission while preserving a reasonably smooth profile.

One or more non-axisymmetric perturbations are then added to $\psi_{h,0}$, resulting in the formation of magnetic islands and modifications to the flux surface shape. It is assumed in these studies that the emission in the presence of these features remains the same function of helical flux as before; the emission is further assumed to be constant within a magnetic island. Finally, the emission is integrated along the USXR array lines-of-sight for multiple toroidal phases of the applied perturbation, simulating plasma rotation and providing a direct comparison to the measured emission fluctuations.

In order to create a magnetic island, a perturbation of the following form is added to the equilibrium helical flux (See the appendix of Ref. [Menard 2005] for details regarding this island model):

$$\partial\psi_h \propto \rho^m (1-\rho)^{m(1-\rho_S)\rho_S} \cos(n\phi - m\theta) \qquad \text{(X)}$$

In order to fix the amplitude of the perturbation, and thus the width of the magnetic island, a time is chosen when the Thomson Scattering (TS) electron temperature profiles show a clear flat spot at the location of the q=2 surface. Of course, not every TS time slice will have the TS viewing locations overlapping the O-point of the magnetic island. However, for cases where the duration of the rotating NTM is >100ms, it is generally found that one of the MPTS time-slices

will demonstrate strong flattening. One such time slice is shown in Fig 9a), where the flat region in the T_e profile spans 1.25<R<1.34 (the predicted location of the q=2 surface is R=1.3 meters in this case). The perturbation amplitude, and thus island width was then adjusted to match this measured width, as shown in frame b).

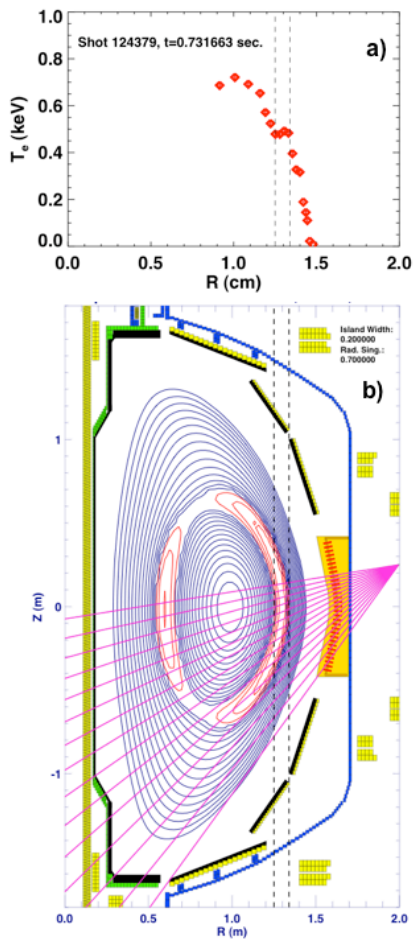

Fig 9. a) Simulated USXR island eigenfunction, and b) T_e profile data used to constrain the magnetic island width.

A comparison between the measured and simulated chord-average emission is shown in Fig. 10. Note that the DC level has been removed in all cases. The measurement in Fig. 10a) shows an inversion layer across chord #4, as expected given this chords near tangency to the q=2 surface. However, there is an additional inversion layer across the magnetic axis, which is incompatible with the emission being due to a purely odd-m mode.

The simulated emission in Fig 10b), derived from the island model described above, also shows the inversion-layer across chord 4. Furthermore, the emission oscillation amplitude on either side of the inversion layer in the simulation is comparable to that in the measurement. Hence, this aspect of the simulation tends to confirm the island eigenfunction in Fig. 9b). However, the simulated emission for chords 7-14 are totally inconsistent with the

measurements: the simulated inversion layer predicted near chord 9 is not present in the measurement, while the measured inversion layer across the magnetic axis is not present in the simulation.

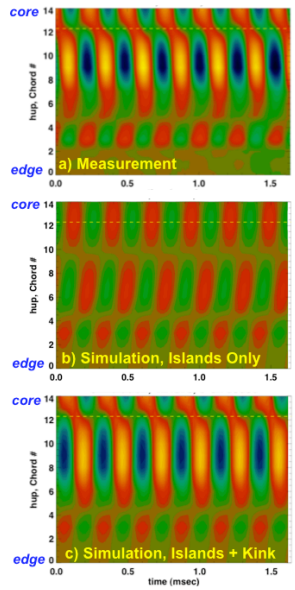

Fig 10. Measured (a) and simulated USXR emission, assuming a 2/1 island only (b), or an island coupled to a 1/1 ideal kink (c). The yellow dashed line indicates the approximate magnetic axis location and the color scales are identical. While both models can achieve good agreement with measurements for the outer chords (0-7), only the 2/1+1/1 model simulates the core emission fluctuation correctly.

In order to resolve this disagreement, an ideal m/n=1/1 perturbation to the plasma core with the following form was added to the already perturbed equilibrium:

$$\xi_{1,1} = \begin{cases} \xi_0 & r < r_c \\ \xi_0 e^{-\left[(r-r_c)/r_f\right]^2} & r > r_c \end{cases} \qquad \text{(X)}$$

Here r_c, r_f, and ξ_0 are parameters to be adjusted. Note that the 1/1 perturbation "rotates" around the plasma magnetic axis twice as fast as the 2/1 island. The phase of the kink and island perturbations was chosen such that the kink perturbation is a radial outward shift at the midplane when the island X-point is at the outboard midplane. When the parameters r_c, r_f and ξ_0 of this 1/1 kink are correctly chosen, the measured and simulated emission patterns can be made to agree quite well, as illustrated by comparing Fig. 10c) to Fig 10a). The coupled mode structures are illustrated in Fig. 11. In the case shown here, the typical shift of the core is ~4 cm, while the island full width at the outboard midplane is ~9cm. We caution, however, that the actual core-eigenfunction could be more complicated than that given by eqn. (X); this form for the core mode should be interpreted as only a simple mode which is consistent with the measure emission fluctuations.

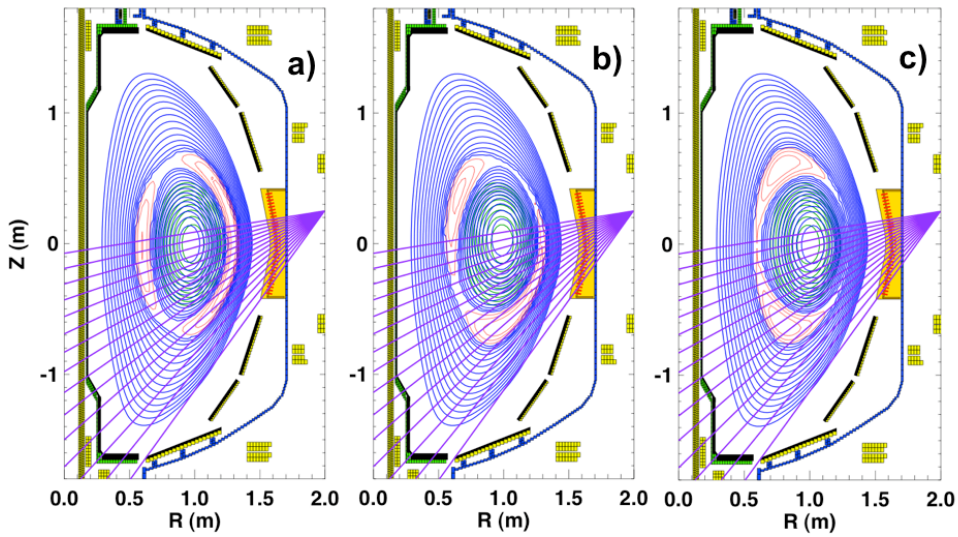

Fig 11. Eigenfunctions of the coupled m/n=1/1 + 2/1 modes. The blue curves represent the nested surfaces of the perturbed equilibrium, the red curves are the surfaces internal to the islands, and the green curves are the core surfaces of the unperturbed equilibrium. The latter are included in order to illustrate the core 1/1 mode more clearly.

Fig. 12 illustrates that the frequency of the coupled modes, as determined from the odd-n Mirnov signal (shown in red), is in near perfect agreement with that determined from the core USXR signal (shown in blue). The signals are plotted from the earliest time when the mode amplitudes are large enough for zero-crossing analysis. This time is generally somewhat earlier for the Mirnov sensors than the USXR chords. Chord 9 from the USXR system is chosen for the analysis, as inspection of the data in Fig. 12 shows that it‘s signal is likely to be dominated by the core 1/1 mode. Also shown are the core and q=2 rotation frequencies. Examples are shown for all three types of triggers.

The key observation is that the 1/1 and 2/1 modes are absolutely locked to each other, for all times and trigger types. This is even true for the ELM trigger case, where the initial frequency is much less that the core or q=2 frequency. As described in detail in Sect. 2.4 of Ref. [Menard 2005], the differential rotation between the core plasma and the MHD perturbation leads to large damping of the core plasma rotation from neoclassical toroidal viscosity (NTV) [Lazzaro 2002], which tends tend to bring the plasma to a state of rigid rotation inside the radius of the large perturbations. Interaction of the island with static error fields or the resistive wall could then lead to further damping of the plasma rotation.

This coupling of 1/1 & 2/1 modes is quite common in NSTX, and represents an additional means for the plasma performance to be deleteriously impacted. In addition to the damping physics noted above and described in detail in Ref. [Menard 2005], these coupled modes can impact the plasma performance in other ways. For instance, these core-modes can lead to fast ion redistribution [Menard 2005, Menard 2007]. This can be deleterious in some contexts (for instance, by reducing the NBI torque), but may be advantageous in maintaining a core safety factor >1. [Menard 2007]. Note also that the coupling of m/n NTMs to

m-1/n modes has previously been reported in ASDEX-Upgrade [Gude 1999, Meskat 2001] and TFTR [Fredrickson 2002].

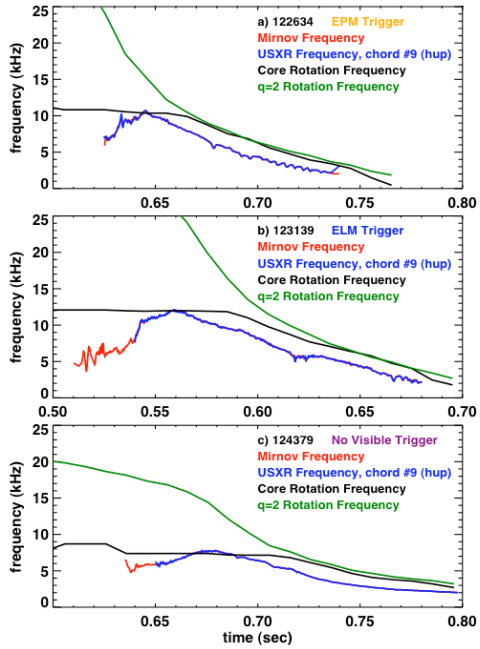

Fig 12. Overlays of the frequency evolution of the odd=n Mirnov frequency (red), the filtered core USXR frequency (blue), and the core (green) and q=2 (black) rotation. See text for more details.

6: Onset Thresholds vs. Rotation, Rotation Shear, and Trigger Type

As indicated from the discussions in Sect. 4, it is clear that the initial mode frequency is a strong function of the triggering mechanism. This observation is reinforced by the observation in Fig 12a.), where the mode frequency at onset is plotted against the q=2 rotation frequency at that time. The mode frequency is determined by an algorithm that tracks the zero-crossings of the filtered odd-n Mirnov signal. For the EPM cases indicated by orange points, the modes can trigger with frequencies either above or below the local rotation frequency. The ELM triggered cases are typically traveling significantly slower than the q=2 rotation at mode onset, and the triggerless case only slightly slower than q=2. The inset to that figure shows the mode frequency at onset plotted against the core rotation frequency at the same time; these two quantities are clearly unrelated.

The same analysis is shown in Fig. 12b), but for a later time when the mode amplitude has saturated. The match between the q=2 surface rotation and the mode frequency is excellent in this case, providing confidence in the reconstruction and analysis methods. The match between the mode and core rotation frequencies is shown in the inset, demonstrating again that the core slows dramatically once the mode strikes.

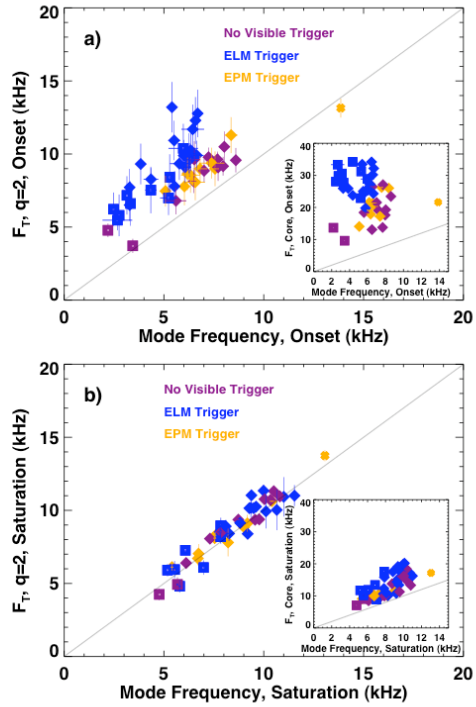

Fig 13. Mode frequency at a) onset and b) saturation, compared to the q=2 frequency. The insets show the mode frequency vs. the core rotation frequency. The colors correspond to different trigger types, while the symbols correspond to different magnetic braking schemes.

As noted in Sect. 2, the polarization threshold mechanism is a function of the island propagation frequency in the E_R=0 rest-frame: $\Omega = \omega_{Mirnov} - \omega_{E_R=0}$. Following Ref. [La Haye 2003], we utilize the NSTX CHERS diagnostic to compute the frequency of the E_R=0 frame as

$$f_{E_R=0} = -\frac{nV_{\phi,j}}{2\pi R} + \frac{n}{2\pi R Z_j e n_j B_\theta}\frac{dp_j}{dr} \qquad \text{(X)}$$

Note that NSTX did not have a measurement of poloidal rotation for these discharges, so the $\frac{nV_{\theta,j}(B_\phi/B_\theta)}{2\pi R}$ term is not included in the present analysis. However, subsequent measurements of V_θ in similar discharges show it to be in the vicinity of 5-10 km/s in these type of plasmas, compared to V_ϕ of typically 50 km/s. Hence, for B_ϕ/B_θ~1 as in an ST, this would be a small correction to the calculation in (X). Furthermore, the $\frac{dp_j}{dr}$ term is generally a small correction to the dominant $\frac{nV_{\phi,j}}{2\pi R}$ term. The diamagnetic frequencies, defined as $\omega_j^* = \vec{k}\cdot\vec{V}_D = \frac{m}{r}V_{D,\theta} + \frac{n}{R}V_{D,\phi}$ with $V_{D,j} = (B\times\nabla p_j)/eZ_j n_j B^2$, are calculated for j={e,i} as

$$\omega_j^* = \vec{k}\cdot\vec{V}_D = \left(\frac{m\langle B_\phi\rangle}{r} - \frac{n\langle B_\theta\rangle}{R}\right)\frac{dp_j}{dr}\frac{1}{Z_j n_j B^2} \qquad \text{(X)}$$

The outcome of this analysis is shown in Fig. 14, where the required NTM drive at mode onset is plotted against the normalized propagation frequency.

This term is expected to be most stabilizing at $\Omega/\omega_i^* = 0.5$, and destabilizing for $\Omega/\omega_i^* < 0$. However, as in DIII-D [Buttery 2008], no clear trend is observed. Thus, it is necessary to look for other trends that might determine the onset threshold.

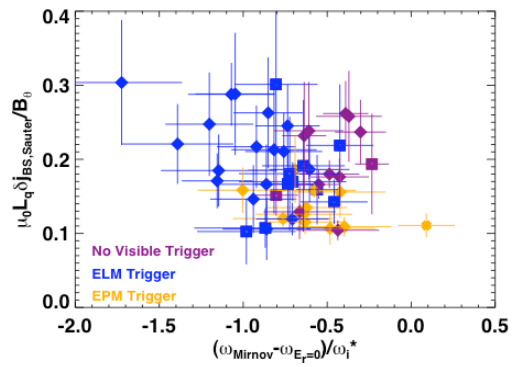

Fig 14. The NTM drive at onset, as a function of the rotation frequency in the E_r=0 frame. No clear trend is apparent.

While figure 14 demonstrates that the local NTM drive is not a function of the mode frequency in the E_R=0 frame, Fig. 15 a) demonstrates that the NTM drive at onset is not a strong function of the lab-frame frequency either. The ELM triggered points (blue) do indeed show a trend of increased drive required at high rotation, though with great scatter. The EPM triggered and trigger-free modes, however, show no clear trend with rotation. The lack of correlation between onset drive and rotation frequency is manifest in the very low linear correlation coefficients indicated in the figure. These and other correlation coefficients are listed in Table 2.

	All Cases	EPM Triggered	ELM Triggered	"Triggerless"
F_T @ q=2	0.10	0.05	0.40	0.00
dF_T/dr @ q=2	0.07	0.01	0.15	0.02
$L_s\tau_A(dF_T/dr)$	**0.45**	**0.61**	**0.61**	**0.45**
$(F_{T,q=2}-F_{T,q=3})$	0.02	0.00	0.41	0.17
$\tau_A^{2/5}\tau_R^{3/5}(F_{T,q=2}-F_{T,q=3})$	0.19	0.00	0.42	0.18
$\tau_A^{2/5}\tau_R^{3/5}(F_{T,q=2}-F_{T,Ped})$	---	---	0.403	---
$\tau_A^{2/5}\tau_R^{3/5}(F_{T,core}-F_{T,q=2})$	---	0.01	---	---

Table 2. Correlation coefficients (r^2) of $\frac{\mu_0 L_q \delta j_{BS}}{B_\theta}$ with various measures of rotation or rotation shear, for both the entire data-set and separated by onset condition. The best correlations are highlighted with bold fonts.

The same onset data, but plotted against rotation shear, is shown in Fig 15b). The improved correlation is immediately apparent, both through visual inspection of the data and in the correlation coefficients. For the EPM triggered and triggerless cases, the correlation coefficient increases from essentially zero

to r^2=0.608 and 0.421 respectively. The increase in correlation for the ELM-triggered cases in blue is not as dramatic, due to the co-linearity between rotation and rotation shear for those cases [see Fig. 4b], but is still statistically significant. In general, when comparing within the different trigger types or the data set as a whole, the NTM drive at onset is better correlated with rotation shear than rotation. Table 1 repeats these correlation coefficients, as well as the correlation with *un-normalized* flow shear; it is clear that the $\tau_A L_S$ normalization is important for achieving the present good correlation.

In addition to the correlation coefficients, linear fit lines are also draw in Fig 14b). The slopes for the EPM-triggered, ELM-triggered, and trigger-free lines are 0.16±.05, 0.2±.04, and 0.26±0.09, respectively. Hence, within the rather large error estimates, the three different trigger types show a similar dependence on rotation shear, a commonality that seems to imply that rotation shear is not impacting the trigger mechanisms directly. Note that the linear fits here do not necessarily imply that the underlying physics has a linear dependence on flow shear. Rather they simply reflect the fact that higher order fits cannot be justified by the data alone, given the number of points and relative scatter.

The data in Fig. 15 b) also shows that for fixed rotation shear, the EPM-triggered modes tend to appear at the lowest levels of NTM drive, and the trigger-less modes at the highest drive levels. The ELM triggered-cases appear at intermediate levels of drive. Note that a similar observation was made of 3/2 NTMs in AUG [Gude 1999], where sawtooth triggered modes had the lowest threshold, followed by fishbone triggered modes and then modes with no apparent trigger.

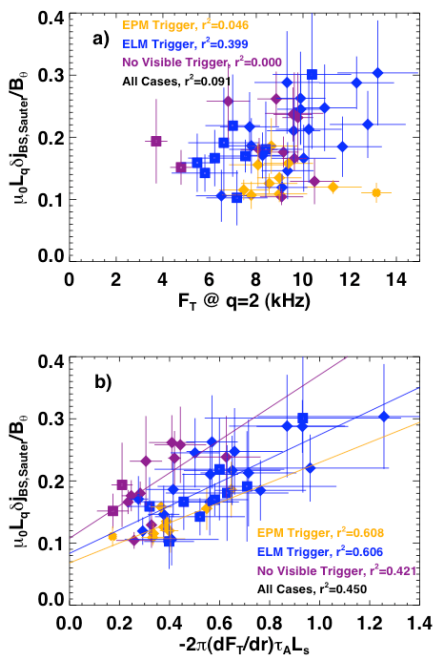

Fig 15. Comparison of the NTM onset drive with a) rotation and b) rotation shear at q=2.

It is observed that the correlation between drive and flow shear is considerable worse for the “triggerless” modes than other cases. If these modes are indeed classically unstable with no trigger, then it is anticipated that the onset

would be very sensitive to parameters beyond only flow shear, including the proximity of q_0 to 1 [Brennan 2007] and β_N to the ideal kink limit [Brennan 2002, Brennan 2003, Brennan 2005]. Hence, the rotation effects are likely only one of many mechanisms determining the onset.

7: Discussion

As was noted in Sect. 2, a possible source for a rotation dependence of the onset threshold is from increased dynamic shielding with increasing differential rotation between the triggering and rational surface. For the cases here, one might expect that the differential rotation between the q=2 surface and the edge would effect the ELM triggered onset, while that between the q=2 surface and the plasma core would might effect the EPM triggered cases. An analysis along these lines is presented in Fig. 16. Frame a) shows the onset NTM drive for the ELM triggered cases, plotted against the differential rotation between the q=2 surface and the pedestal top. The differential rotation here and in the following discussion is normalized to the tearing time $\tau_A^{2/5}\,\tau_R^{3/5}$ [La Hay 2000]. The pedestal is defined here to be 4 cm inside the outboard separatrix, as determined by EFIT [Sabbagh 2001]. Note that the database has significant colinearity between this difference frequency and the local toroidal flow shear at q=2. However, the correlation between the onset drive with local rotation shear is significantly better than the correlation with q=2/edge differential rotation.

A similar conclusion can be drawn from Fig. 16b), where the onset NTM drive for EPM triggered modes is plotted against the q=2/core differential rotation. As described in Sect. 4, USXR analysis indicates that these triggering modes are often localized to the core of the plasma. The correlation between the onset drive and q=2/core differential rotation is quite poor. Hence, we infer that for both the ELM and EPM triggered modes, differential rotation between the triggering surface and the NTM rational surface is unlikely to be the dominant effect in setting the drive threshold.

In the late 1980s and early 1990s, a series of investigations of tearing mode (TM) stability in slab geometry were carried out [Einaudi 1986, Einaudi 1989, Chen 1990 A, Chen 1990 B, Ofman 1993]. The inviscid numerical modeling of the linear TM in Ref. [Einaudi 1986] showed that for small values of flow shear, the growth rate of the mode increased as the flow shear increased. However, for flow shear larger compared to magnetic shear, the TM was either stabilized or became a Kelvin-Helmholtz like mode modified by magnetic shear, depending of the parity of the flow profile across the magnetic null line. This work was extended to include viscosity in Ref. [Einaudi 1989], where it was confirmed that for the TM without flow shear, viscosity slowed the mode growth. However, depending on the magnitudes of the flow compared to the Alfven velocity and the flow shear length compared to the magnetic shear length, viscosity could be either stabilizing or destabilizing. In the inviscid modeling of the linear TM in Ref. [Chen 1990 A], it was emphasized that flow shear could modify tearing stability through changes to both the inner resistive layer and outer ideal region. For flow shear small compared to magnetic shear, the TM was destabilized, while flow shear large compared to magnetic shear lead to TM stabilization. These studies

were also extended to include viscosity [Chen 1990 B], where for small flow shear, it was demonstrated that viscosity slowed the mode growth, but did not stabilize it. Furthermore, it was confirmed that the TM was still suppressed when flow shear dominated magnetic shear. Finally, a numerical study of the nonlinear evolution of the TM was presented in Ref. [Ofman 1993]. It was demonstrated that shear-flow reduced the magnetic island width, though the extent of the reduction depended on the details of the flow profile.

In the full toroidal simulation in Ref. [Chandra 2005, Sen 2005], the effects of rotation shear at the rational surface and differential rotation between surfaces on the stability of the TMs and NTMs was studied. For the classical tearing mode, it was demonstrated that small positive rotation shear is destabilizing, in agreement with the analytic modeling noted above [Chen 1990 A], while negative rotation shear is stabilizing [Sen 2005]. Differential rotation, on the other hand, was found to be stabilizing, due to both enhancements of the pressure-curvature term and reduced coupling between the TM rational surfaces. Also, the stabilizing pressure-curvature term increased, due to flow-induced changes in the equilibrium. Similar effects were found for the classically stable NTM case. Note, however, that these simulations were done for Alfven mach-numbers significantly smaller than in NSTX.

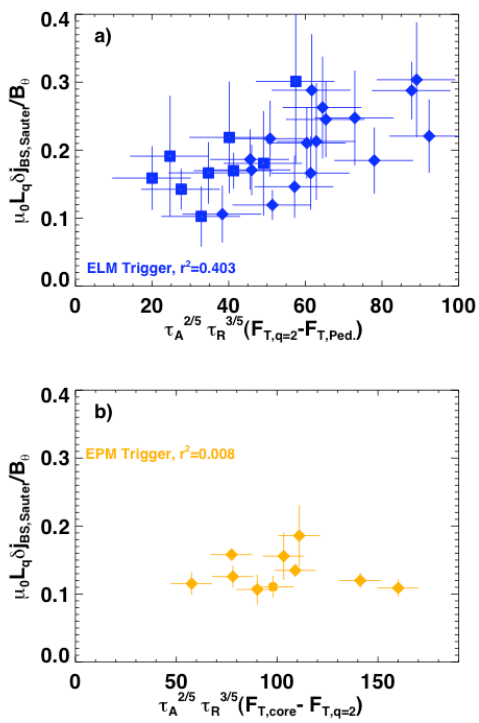

Fig 16. Comparison of NTM drive at mode onset with differential rotation: a) Difference between q=2 and pedestal rotation, for ELM triggered modes, and b) difference between core and q=2 rotation, for EPM triggered modes. The correlation coefficients are plotted as well, for comparison with those in Fig. 14.

In order to asses a possible dependence on differential rotation between rational surfaces, the NTM drive at mode onset is plotted in Fig 17, as a function of the differential rotation between the q=2 and q=3 surfaces, where the

frequency difference is again normalized to the tearing time. For NSTX profiles, the there is strong co-linearity between this differential rotation and the local rotation shear. Nevertheless, the degree of correlation is reduced in Fig. 17 compared to the correlation with local flow shear. Note that there is no q=1 surface in the plasma in these cases.

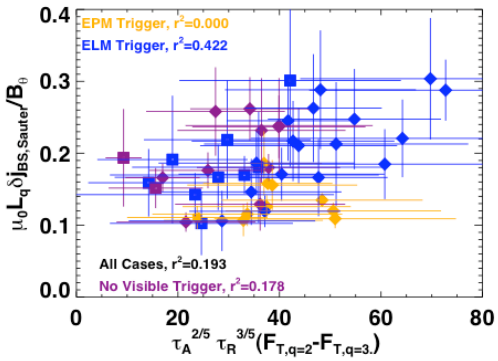

Fig 17. Comparison of the NTM drive at mode turn on, as a function of the differential rotation between then q=3 and q=2 surfaces.

The same authors also utilized a generalized Newcomb equation to study the effects of flow shear on the classical TM in cylindrical geometry [Chandra 2007]. This model in particular shows that flow shear can be stabilizing to the TM, depending on the shear in both the magnetic field and velocity profiles.

A final important study was presented by Coelho and Lazzaro [Coelho 2007], again for the classical linear TM in low-β cylindrical geometry with toroidal rotation shear. It was found that flow shear is destabilizing in a plasma without viscosity, but stabilizing for large values of viscosity. It was demonstrated that for flow shear exceeding a threshold value, an otherwise unstable TM could be stabilized; that threshold depended on the ratio of the resistive time to the viscous time (the Prandtl number).

In summary, this brief survey above demonstrates that there is rich physics involved in the stability properties of TMs/NTMs in the presence of flow. Many of these theoretical/numerical results are encouraging in light of the NSTX data, in that they show means by which flow shear can be stabilizing for the TM. However, given that only one of these calculations was done in toroidal geometry with neoclassical destabilization [Chandra 2005], and that it indicated a destabilizing effect of flow shear on the NTM, it is clear that further theory and modeling is required in order to understand the NSTX results presented in this manuscript.

8: Summary

This paper has focused on the m/n=2/1 neoclassical tearing mode in the spherical torus NSTX. Important conclusions include:

- There are at least three mechanisms by which the mode is triggered: EPM triggers, ELM triggers, and cases where there is no apparent trigger.

These cases are easily distinguished by the D_α emission, D-D neutron emission, and frequency evolution just after mode initiation.

- The 2/1 island appears to be coupled to a 1/1 core mode in essentially all cases, as was seen in ASDEX-Upgrade [Gude 1999] and TFTR [Fredrickson 2002]. The effects of this core mode on the 2/1 mode stability are as yet unstudied. However, this core modes contributes strongly to the observed plasma rotation damping [Menard 2005].

- Although there can be a substantial frequency difference between the mode and the q=2 rotation and mode initiation, there is no trend to imply that the polarization threshold provides a rotation dependence for the NTM drive at onset.

- The NTM drive at mode onset is highly correlated with the local rotation shear. This is true for entire data-set, and when the data-set is broken into different trigger mechanisms.

- For fixed rotation shear, the EPM triggered modes are initiated at the lowest level of NTM drive and the “triggerless” cases at the highest drive levels. The ELM triggered cases onset at intermediate levels of NTM drive.

- A review of the published literature shows that mechanisms related to both flow shear and differential flow are possible candidates for the observed trends. However, as the simulations typically do not match NSTX conditions and the data has not-insignificant scatter, it is as yet difficult to pin down the exact mechanism.

These conclusions lead to many clear research tasks for future study. A high priority is to do simulations with the relevant geometry, flow profiles, and plasma parameters. These simulations will hopefully elucidate the importance of various effects described in Sect. 7 (toroidal coupling, viscosity, enhancement of the pressure-curvature term). Additionally, addressing the influence of the coupled 1/1 mode on the 2/1 mode stability is important for understanding the dynamics of these discharges.

Experimentally, an important task is the learn to operate NSTX without these deleterious modes. The use of ECCD to stabilize m/n=2/1 NTMs by driving current in the island is now established in DIII-D [Petty 2004, Prater 2007], JT-60 [Isayama 2008] and AUG [Maraschek 2005], and is planned for NTM stabilization in ITER [Hender 2007, La Haye 2008 B]. This technology is not available in NSTX, due to the low magnetic field and high density, and other control techniques must be sought. One clear option is to maintain $q_{min}>2$, although the deleterious effects of m/n=3/1 modes must then be addressed. Another option becomes apparent from the work in Ref. [Warrick 2000], where lower-hybrid current drive was utilized to modify the current profile in order to make Δ' more

negative. If future STs have flexible neutral beam current drive systems, similar manipulation of the current profile might be possible, opening a route to stabilization with q_{min}<2.

9: Acknowledgements

This research was funded by the United States Department of Energy. The authors are grateful to the members of the NSTX team for their assistance in executing these experiments and the associated analysis.

Appendix: Comparison of the various bootstrap current definitions.

The definition of bootstrap drive utilized in this paper, Eqn. (1) is based on a formulation of the bootstrap current that is accurate over a variety of plasma shapes and aspect ratios [Sauter 1999]. However, many studies of NTMs have utilized simplified large-aspect ratio formula. It is the purpose of this appendix to compare these different definitions, in order to clarify the relationship between these and previous results.

Figure A1 a) shows various definitions of the NTM drive terms in the MRE. Two approximations for the drive are plotted against the simplified large-aspect ratio approximation in Eqn. X: the drive using the full Sauter formulation after mapping all variables to poloidal flux (Eqn. X), and a simplified drive using a large aspect ratio approximation to the Sauter model:

$$Drive = -\sqrt{\varepsilon} L_q \beta_{Pe} \left[1.32 \left(1 + {T_i}/{T_e} \right) L_{n_e} + 1.14 L_{T_e} \right] \qquad \text{(X)}$$

It is clear that the two drive definitions based on the Sauter model have very similar values, and tend to be about 20% higher than the simplest definition. Note that some of the scatter is due to differences in how the radial derivatives are calculated in the two formulation. In general, this result indicates that previous work at large aspect ratio formulated in terms of Eqn X. can be directly compared to the present NSTX results.

Fig A1 b) compares the simplified NTM drive term to three other common surrogate for the drive: the global β_N and β_P, as determined by equilibrium reconstruction, and the local electron poloidal-β. It is clear that these simpler definitions do not scale well with the local bootstrap drive; the wide variety of magnetic braking, heating powers, and mode onset times leads to a substantial variety in the local gradients for the present database, and so the full local formulation must be taken into account.

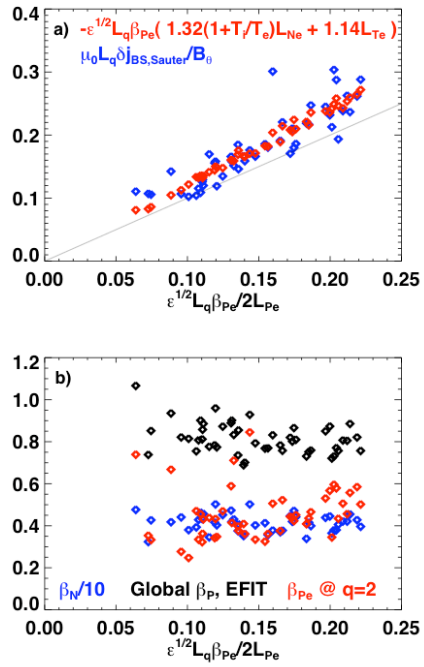

Fig A1. a) Comparison of the simplest bootstrap drive definition with more two implementations of the Sauter model, and b) comparison of the simplest bootstrap drive definition to various global and local β values.

References

[Buttery 2001] R. J. Buttery, T. C. Hender, D. F. Howell, G. T. A. Huysmans, M. Mayoral, S. D. Pinches, A. Pochelon, O. Sauter, H. Wilson, M. Zabiego, and contributors to the EFDA-JET workprogramme, *Proceedings of the 28th EPS Conference on Controlled Fusion and Plasma Physics, Portugal, 2001, European Physical Society Conference Abstract* (Institute of Physics, Bristol, 2001), Vol. 25, p.5.011.

[Buttery 2002] R. Buttery, O. Sauter, R. Akers, M. Gryaznevich, R. Martin, C.D. Warrick, H.R. Wilson, and the MAST Team, Phys. Rev. Lett **88**, 125005 (2002).

[Buttery 2008] R. J. Buttery, R. J. La Haye, P. Gohil, G. L. Jackson, H. Reimerdes, E. J. Strait, and the DIII-D Team, Phys. Plasmas **15**, 056115 (2008).

[Brennan 2002] D. Brennan, E.J. Strait, A.D. Turnbull, M.S. Chu, R.J. La Haye, T.C. Luce, T.S. Taylor, S. Kruger, and A. Pletzer, Phys. Plasmas **9**, 2998 (2002).

[Brennan 2003] D. Brennan, R.J. La Haye, A.D. Turnbull, M.S. Chu, T.H. Jensen, L.L. Lao, T.C Luce, P.A. Politzer, and E.J. Strait, Phys. Plasmas **10**, 1643 (2003).

[Brennan 2005] D. Brennan, S. E. Kruger, T.A. Gianakon, and D.D. Schnack, Nuclear Fusion **45**, 1178 (2005).

[Brennan 2007] D. Brennan, A.D. Turnbull, M.S. Chu, R.J. La Haye, L.L. Lao, T.H. Osborne, and S.A. Galkin, Phys. Plasmas **14**, 06108 (2007).

[Chandra 2005] D. Chandra, A. Sen, P. Kaw, M.P. Bora, and S. Kruger, Nuclear Fusion **45**, 524 (2005).

[Chandra 2007] D. Chandra, A. Sen, and P. Kaw, Nuclear Fusion **47**, 1238 (2007).

[Chang 1990] Z. Chang and J.D. Callen, Nuclear Fusion **30**, 219 (1990).

[Chang 1995] Z. Chang, J.D. Callen, E.D. Fredrickson, R.V. Budny, C.C. Hegna, K.M. McGuire, M.C. Zarnstorff, and the TFTR Group, Phys. Rev. Lett. **74**, 4663 (1995).

[Chen 1990 A] X.L. Chen and P.J. Morrison, Phys. Fluids B **2**, 495 (1990).

[Chen 1990 B] X.L. Chen and P.J. Morrison, Phys. Fluids B **2**, 2574 (1990).

[Coelho 2007] R. Coelho and E. Lazzaro, Phys. Plasmas **14**, 012101 (2007).

[Einaudi 1986] G. Einaudi and F. Rubini, Phys. Fluids **29**, 2563 (1986).

[Einaudi 1989] G. Einaudi and F. Rubini, Phys. Fluids B**, 1**, 2224 (1989).

[Fitzpatrick 1995] R. Fitzpatrick, Phys. Plasmas **2**, 825 (1995).

[Fitzpatrick 1993] R. Fitzpatrick, Nuclear Fusion **33**, 1049 (1993).

[Fredrickson 2002] E. Fredrickson, Phys. Plasmas **9**, 548 (2002).

[Furth 1963] H. P. Furth, J. Killeen, and M.N. Rosenbluth, Phys. Fluids **6**, 459 (1963).

[Furth 1973] H.P. Furth, P.H. Rutherford, and H. Selber, Phys. Fluids **16**, 1054 (1973).

[Gates 1997] D. Gates, B. Lloyd, A.W. Morris, G. McAdrle, M.R. O'Brien, M. Valovic, C. D. Warrick, H.R. Wilson, Compass-D Team, ECRH Team, UKAEA, Nuclear Fusion **37**, 1593 (1997)

[Gates 2006] D. A. Gates, R. Maingi, J. Menard, S. Kaye, S. A. Sabbagh, G. Taylor, J. R. Wilson, M. G. Bell, R. E. Bell, S. Bernabei, J. Bialek, T. Biewer, W. Blanchard, J. Boedo, C. Bush, M. D. Carter, W. Choe, N. Crocker, D. S. Darrow, W. Davis, L. Delgado-Aparicio, S. Diem, J. Ferron, A. Field, J. Foley, E. D. Fredrickson, R. Harvey, R. E. Hatcher, W. Heidbrink, K. Hill, J. C. Hosea, T. R.

Jarboe, D. W. Johnson, R. Kaita, C. Kessel, S. Kubota, H. W. Kugel, J. Lawson, B. P. LeBlanc, K. C. Lee, F. Levinton, J. Manickam, R. Maqueda, R. Marsala, D. Mastrovito, T. K. Mau, S. S. Medley, H. Meyer, D. R. Mikkelsen, D. Mueller, T. Munsat, B. A. Nelson, C. Neumeyer, N. Nishino, M. Ono, H. Park, W. Park, S. Paul, W. Peebles, M. Peng, C. Phillips, A. Pigarov, R. Pinsker, A. Ram, S. Ramakrishnan, R. Raman, D. Rasmussen, M. Redi, M. Rensink, G. Rewoldt, J. Robinson, P. Roney, L. Roquemore, E. Ruskov, P. Ryan, H. Schneider, C. H. Skinner, D. R. Smith, A. Sontag, V. Soukhanovskii, T. Stevenson, D. Stotler, B. Stratton, D. Stutman, D. Swain, E. Synakowski, Y. Takase, K. Tritz, A. von Halle, M. Wade, R. White, J. Wilgen, M. Williams, W. Zhu, S. J. Zweben, R. Akers, P. Beiersdorfer, R. Betti, and T. Bigelow, Phys. Plasmas **13**, 056122 (2006).

[Gerhardt 2009] Short 2/1 Mode Onset Paper

[Glasser 1975] A.H. Glasser, J.M. Greene, and J.L. Johnson, Phys. Fluids **18**, 875 (1975).

[Gude 1999] A. Gude, S. Gunter, S. Sesnic, and the ASDEX Upgrade Team, Nuclear Fusion **39**, 127 (1999).

[Gunter 1998] S. Gunter, A. Gude, M. Maraschek, S. Sesnic, H. Zohm, ASDEX Upgrade Team, Nuclear Fusion **38**, 1431 (1998).

[Hegna 1998] C.C. Hegna, Phys. Plasmas **5**, 1767 (1998).

[Hegna 1999] C.C. Hegna, J.D. Callen, and R. J. La Haye, Phys Plasmas **6**, 130 (1999).

[Hender 2004] T.C. Hender, D.F. Howell, R.J. Buttery, O. Sauter, F. Sartori, R.J. LaHaye, A.W. Hyatt, C.C. Petty, JET EFDA contributors, and the DIII-D team, Nuclear Fusion **44**, 788 (2004).

[Hender 2007] T.C. Hender, J.C Wesley, J. Bialek, A. Bondeson, A.H. Boozer, R.J. Buttery, A. Garofalo, T.P Goodman, R.S. Granetz, Y. Gribov, O. Gruber, M. Gryaznevich, G. Giruzzi, S. Günter, N. Hayashi, P. Helander, C.C. Hegna, D.F. Howell, D.A. Humphreys, G.T.A. Huysmans, A.W. Hyatt, A. Isayama, S.C. Jardin, Y. Kawano, A. Kellman, C. Kessel, H.R. Koslowski, R.J. La Haye, E. Lazzaro, Y.Q. Liu, V. Lukash, J. Manickam, S. Medvedev, V. Mertens, S.V. Mirnov, Y. Nakamura, G. Navratil, M. Okabayashi, T. Ozeki, R. Paccagnella, G. Pautasso, F. Porcelli, V.D. Pustovitov, V. Riccardo, M. Sato, O. Sauter, M.J. Schaffer, M. Shimada, P. Sonato, E.J. Strait, M. Sugihara, M. Takechi, A.D. Turnbull, E. Westerhof, D.G. Whyte, R. Yoshino, H. Zohm and the ITPA MHD, Disruption and Magnetic Control Topical Group, Nuclear Fusion **47**, S128 (2007).

[Huysmans 1999] JET Team, Nuclear Fusion **39**, 1965 (1999).

[Isayama 2008] A. Isayama, G. Matsunaga, T. Kobayashi, S. Moriyama, N. Oyama, Y. Sakamoto, T. Suzuki, H. Urano, N. Hayashi, Y. Kamada, T. Ozeki, Y. Hirano, L. Urso, H. Zohm, M. Maraschek, J. Hobirk, K. Nagasaki, and the JT-60 team, in Fusion Energy 2008 (Proc. 22th Int. Conf. Geneva, 2008) (Vienna: IAEA) CD-ROM file EX/5-4

[Itoh 2002] S.-I. Itoh, K. Itoh, and M. Yagi, Phys. Rev. Lett **91**, 045003 (2003).

[Itoh 2004] S.-I. Itoh, K. Itoh, and M. Yagi, Plasma Phys. Control. Fusion **46**, 123 (2004).

[Joffrin 2003] E Joffrin, F Crisanti, R Felton, X Litaudon, D Mazon, D Moreau, L Zabeo, R Albanese, M Ariola, D Alves, O Barana, V Basiuk, A Bécoulet, M Bécoulet, J Blum, T Bolzonnella, K Bosak, J M Chareau, M de Baar, E de la Luna, P de Vries, P Dumortier, D Elbeze, J Farthing, H Fernandes, C Fenzi, R Giannella, K Guenther, J Harling, N Hawkes, T C Hender, D F Howell, P Heesterman, F Imbeaux, P Innocente, L Laborde, G Lloyd, P J Lomas, D C McDonald, J Mailloux, M Mantsinen, A Messiaen, A Murari, J Ongena, F Orsitto, V Pericoli-Ridolfini, M Riva, J Sanchez, F Sartori, O Sauter, A C C Sips, T Tala, A Tuccillo, D Van Ester, K-D Zastrow, M Zerbini and contributors to the JET EFDA Programme, Plasma Phys. Control Fusion **45**, A367 (2003).

[Kruger 1998] S. Kruger, C.C. Hegna, and J.D. Callen, Phys. Plasmas **5**, 455 (1998).

[Lazzaro 2002] E. Lazzaro ,R. J. Buttery and T. C. Hender, P. Zanca, R. Fitzpatrick, M. Bigi, T. Bolzonella, R. Coelho, M. DeBenedetti, S. Nowak, O. Sauter, M. Stamp and contributors to the EFDA-JET work programme, Phys. Plasmas **9**, 3906 (2002)

[La Haye 1997] R.J. LaHaye, L.L. Lao, E.J. Strait, and T.S. Taylor, Nuclear Fusion **37**, 397 (1997)

[La Haye 2000] R. J. La Haye, R.J. Buttery, S. Guenter, G.T.A. Huysmans, M. Maraschek, and H.R. Wilson, Phys. Plasmas **7**, 3349 (2000).

[La Haye 2003] R. J. La Haye, C. C. Petty, E. J. Strait, F. L. Waelbroeck, and H. R. Wilson, Phys. Plasmas **10**, 3644 (2003).

[La Haye 2006] R.J. La Haye, Phys. Plasmas **13**, 055501 (2006).

[La Haye 2008 A] R. J. LaHaye, P.A. Politzer, and D.P. Brennan, Nuclear Fusion **48**, 015005 (2008).

[La Haye 2008 B] R. J. LaHaye, J.R. Ferron, D. A. Humphreys, T.C. Luce, C.C. Petty, R. Prater, E.J. Strait, and A.S. Welander, Nuclear Fusion **48**, 054004 (2008).

[Le Blanc 2003] B.P. LeBlanc, R.E. Bell, D. W. Johnson, D.E. Hoffman, D.C. Long, and R.W. Palladino, Rev. Sci. Instrum. **74**, 784 (2001)

[Luce 2001] T.C. Luce, M.R. Wade, P.A. Politzer, S.L. Allen, M.E. Austin, D.R. Baker, B. Bray, D.P. Brennan, K.H. Burrell, T.A. Casper, M.S. Chu, J.C. DeBoo, E.J. Doyle, J.R. Ferron, A.M. Garofalo, P. Gohil, I.A. Gorelov, C.M. Greenfield, R.J. Groebner, W.W. Heidbrink, C.-L. Hsieh, A.W. Hyatt, R. Jayakumar, J.E. Kinsey, R.J. La Haye, L.L. Lao, C.J. Lasnier, E.A. Lazarus, A.W. Leonard, Y.R. Lin-Liu, J. Lohr, M.A. Mahdavi, M.A. Makowski, M. Murakami, C.C. Petty, R.I. Pinsker, R. Prater, C.L. Rettig, T.L. Rhodes, B.W. Rice, E.J. Strait, T.S. Taylor, D.M. Thomas, A.D. Turnbull, J.G. Watkins, W.P. West and K.-L. Wong, Nuclear Fusion **41**, 1585 (2001).

[Maraschek 2005] M. Maraschek, G. Gantenbein, T.P. Goodman, S. G Gunter, D.F. Howell , F. Leuterer1 , A. M Muck1 , O. Sauter3 , H. Zohm1 , Contributors to the EFDA-JET Workprogramme and the ASDEX Upgrade Team, Nuclear Fusion **45**, 1369 (2005)

[Menard 2005] J.E. Menard, R.E. Bell, E.D. Fredrickson, D.A. Gates, S.M. Kaye, B.P. LeBlanc, R. Maingi, S.S. Medley, W. Park, S.A. Sabbagh, A. Sontag, D. Stutman, K. Tritz, W. Zhu and the NSTX Research Team, Nuclear Fusion **45**, 539 (2005).

[Menard 2007] J.E. Menard, R.E. Bell, D.A. Gates, S.M. Kaye, B.P. LeBlanc, F.M. Levington, S.S. Medley, S.A. Sabbagh, D. Stutman, K. Tritz, and H. Yuh, Phys. Rev. Lett, **97**, 095002 (2006).

[Meskat 2001] J.P. Meskat, H. Zohm, G. Gantenbein, S. Gunter, M. Maraschek, W. Suttop, Q. Yu, and the ASDEX Upgrade Team, Plasma Phys. Control. Fusion **43**, 1325 (2001).

[Najmabadi 2003] F. Najmabadi and the ARIES Team, Fusion Engineering and Design **65**, 141 (2003).

[Ofman 1993] L. Ofman, P.J. Morrison, and R.S. Steinolfson, Phys. Fluids B **5**, 376 (1993).

[Ono 2000] M. Ono, S. M. Kaye, Y.-K.M. Peng, G. Barnes, W. Blanchard, M.D. Carter, J. Chrzanowski, L. Dudek, R. Ewig, D. Gates, R.E. Hatcher, T. Jarboe, S.C. Jardin, D. Johnson, R. Kaita, M. Kalish, C.E. Kesel, H. W. Kugel, R. Maingi, R. Majeski, J. Manickam, B. McCormack, J. Menard, D. Mueller, B.A. Nelson, B.E. Nelson, C. Neumeyer, G. Oliaro, F. Paoletti, R. Parsells, E. Perry, N.

Pomphrey, S. Ramakrishnan, R. Raman, G. Rewoldt, J. Robinson, A.L. Roquemore, P. Ryan, S. Sabbagh, D. Swain, E.J. Synakowski, M. Viola, M. Williams, J.R. Wilson, and the NSTX Team, Nuclear Fusion **40**, 557 (2000).

[Peng 1986] Y.K.M. Peng and D.J. Strickler, Nuclear Fusion **26**, 769 (1986).

[Peng 2008] Y.K.M. Peng, T.W. Burgess, A.J. Carroll, C.L. Neumeyer, J.M. Canik, M.J. Cole, W.D. Dorland, P.J. Fogarty, L. Grisham, D.L. Hillis, Y. Katoh, K. Korsah, M. Kotschenreuther, R. LaHaye, S. Mahajan, R. Majeski, B.E. Nelson, B.D. Patton, D.A. Rasmussen, S.A. Sabbagh, A.C. Sontag, R.E. Stoller, C.-C. Tsai, P. Valanju, J.C. Wagner, G.L. Yoder, in Fusion Energy 2008 (Proc. 22th Int. Conf. Geneva, 2008) (Vienna: IAEA) CD-ROM file FT/P3-14

[Peng 2005] Y-K M Peng , P J Fogarty, T W Burgess, D J Strickler, B E Nelson, J Tsai, C A Neumeyer, R Bell, C Kessel, J Menard, D Gates, B LeBlanc, D Mikkelsen, E Fredrickson, L Grisham, J Schmidt, P Rutherford, S Sabbagh, A Field, A Sykes, I Cook, O Mitarai, and Y Takase, Nuclear Fusion **47**, B263 (2005).

[Peters 2000] A.G. Peters, Plasma Phys. Control. Fusion **42**, 2000 (B231).

[Petty 2005] C.C. Petty, R.J. La Haye, T.C. Luce, D.A. Humphreys, A.W. Hyatt, J. Lohr, R. Prater, E.J. Strait and M.R. Wade, Nuclear Fusion **44**, 243 (2004)

[Poli 2002] E. Poli, A.G. Peeters, A. Bergmann, S. Gunter, and S.D. Pinches, Phys. Rev. Lett. **88**, 075001 (2002).

[Prater 2007] R. Prater, R.J. La Haye, T.C. Luce, C.C. Petty, E.J. Strait, J.R. Ferron , D.A. Humphreys , A. Isayama , J. Lohr , K. Nagasaki , P.A. Politzer, M.R. Wade and A.S. Welander, Nuclear Fusion **47**, 371 (2007).

[Reimerdes 1] H. Reimerdes, O. Sauter, T. Goodman, and A. Pochelon, Phys. Rev. Lett **88**, 105005 (2002).

[Ren 1998] C. Ren, J.D. Callen, T.A. Gianakon, C.C. Hegna, Z. Chang, E.D. Fredrickson, K.M. McGuire, G. Taylor, and M.C. Zarnstorff, Phys. Plasmas **5**, 450 (1998).

[Rutherford 1973] P.H. Rutherford, Phys. Fluids **16**, 1903 (1973).

[Sauter 1997] O. Sauter, R. J. La Haye, Z. Chang, D. A. Gates, Y. Kamada, H. Zohm, A. Bondeson, D. Boucher, J. D. Callen, M. S. Chu, T. A. Gianakon, O. Gruber, R. W. Harvey, C. C. Hegna, L. L. Lao, D. A. Monticello, F. Perkins, A.

Pletzer, A. H. Reiman, M. Rosenbluth, E. J. Strait, T. S. Taylor, A. D. Turnbull, F. Waelbroeck, J. C. Wesley, H. R. Wilson, and R. Yoshino, Phys Plasmas **4**, 1654 (1997).

[Sauter 1999] O. Sauter, C. Angioni, and Y.R. Lin-Liu, Phys. Plasmas **6**, 2834 (1999).

[Sauter 2002] O. Sauter, E. Westerhof, M. L. Mayoral, B. Alper, P. A. Belo, R. J. Buttery, A. Gondhalekar, T. Hellsten, T. C. Hender, D. F. Howell, T. Johnson, P. Lamalle, M. J. Mantsinen, F. Milani, M. F. Nave, F. Nguyen, A. L. Pecquet, S. D. Pinches, S. Podda, and J. Rapp, Phys. Rev. Lett **88**, 105001 (2002).

[Sen 2005] A. Sen, D. Chandra, P. Kaw, M.P. Bora, and S. Kruger, Neoclassical tearing modes in the presence of sheared flows, 32nd EPS Conference on Plasma Physics, Tarragona, Spain (2005).

[Sips 2002] A C C Sips, R Arslanbekov, C Atanasiu, W Becker, G Becker, K Behler, K Behringer, A Bergmann, R Bilato, D Bolshukhin, K Borrass, B Braams, M Brambilla, F Braun, A Buhler, G Conway, D Coster, R Drube, R Dux, S Egorov, T Eich, K Engelhardt, H-U Fahrbach, U Fantz, H Faugel, M Foley, K B Fournier, P Franzen, J C Fuchs, J Gafert, G Gantenbein, O Gehre, A Geier, J Gernhardt, O Gruber, A Gude, S Günter, G Haas, D Hartmann, B Heger, B Heinemann, A Herrmann, J Hobirk, F Hofmeister, H Hohenöcker, L Horton, V Igochine, D Jacobi, M Jakobi, F Jenko, A Kallenbach, O Kardaun, M Kaufmann, A Keller, A Kendl, J-W Kim, K Kirov, R Kochergov, H Kollotzek, W Kraus, K Krieger, B Kurzan, P T Lang, P Lauber, M Laux, F Leuterer, A Lohs, A Lorenz, C Maggi, H Maier, K Mank, M-E Manso, M Maraschek, K F Mast, P McCarthy, D Meisel, H Meister, F Meo, R Merkel, D Merkl, V Mertens, F Monaco, A Mück, H W Müller, M Münich, H Murmann, Y-S Na, G Neu, R Neu, J Neuhauser, J-M Noterdaeme, I Nunes, G Pautasso, A G Peeters, G Pereverzev, S Pinches, E Poli, M Proschek, R Pugno, E Quigley, G Raupp, T Ribeiro, R Riedl, S Riondato V Rohde , J Roth, F Ryter, S Saarelma, W Sandmann, S Schade, H-B Schilling, W Schneider, G Schramm, S Schweizer, B Scott1, U Seidel, F Serra, S Sesnic, C Sihler, A Silva, E Speth, A Stäbler, K-H Steuer, J Stober, B Streibl, E Strumberger, W Suttrop, A Tabasso, A Tanga, G Tardini, C Tichmann, W Treutterer, M Troppmann, P Varela, O Vollmer, D Wagner, U Wenzel, F Wesner, R Wolf, E Wolfrum, E Würsching, Q Yu, D Zasche, T Zehetbauer, H-P Zehrfeld and H Zohm, Plasma Phys. Control. Fusion **44**, B69 (2002).

[Shimada 2007] M. Shimada, D.J. Campbell, V. Mukhovatov, M. Fujiwara N. Kirneva, K. Lackner, M. Nagami, V.D. Pustovitov, N. Uckan, J. Wesley, N. Asakura, A.E. Costley, A.J.H. Donné, E.J. Doyle, A. Fasoli, C. Gormezano, Y. Gribov, O. Gruber, T.C. Hender, W. Houlberg, S. Idei, Y. Kamada, A. Leonard, B. Lipschultz, A. Loarte, K. Miyamoto, V. Mukhovatov, T.H. Osborne, A. Polevoii, and A.C.C. Sips, Nuclear Fusion **47**, S1 (2007).

[Sabbagh 2001] S.A. Sabbagh, S.M. Kaye, J. Menard, F. Paoletti, M. Bell, R.E. Bell, J.M. Bialek, M. Bitter, E.D. Fredrickson, D.A. Gates, A.H. Glasser, H. Kugel, L.L. Lao, B.P. LeBlanc, R. Maingi, R.J. Maqueda, E. Mazzucato, D. Mueller, M. Ono, S.F. Paul, M. Peng, C.H. Skinner, D. Stutman, G.A. Wurden, W. Zhu and NSTX Research Team, Nuclear Fusion **41**, 1601 (2001).

[Stutman 1999] D. Stutman, M. Finkenthal, V. Soukhanovski, M.J. May, H.W. Moss, and R. Kaita, Rev. Sci. Instrum. **70**, 572 (1999).

[Press 1992] W.H. Press, B.P. Flannery, S. A. Teukolsky, and W.T. Vetterling, *Numerical Recipes in C, the Art of Scientific Computing, 2nd- edition*. Cambridege University Press, 1992, Section 18.5.

[Wade 2005] M.R. Wade, T.C. Luce, R.J. Jayakumar, P.A. Politzer, A.W. Hyatt, J.R. Ferron, C.M. Greenfield, M. Murakami, C.C. Petty, R. Prater, J.C. DeBoo, R.J. La Haye, P. Gohil and T.L. Rhodes, Nuclear Fusion **45**, 407 (2005).

[Warrick 2000] C.D. Warrick, R. Buttery, G. Cunningham, S.J. Fielding, T.C. Hender, B. Lloyd, A.W. Morris, M.R. O'Brien, T. Pinfold, K. Stammers, M. Valovic, M. Walsh, H.R. Wilson, and COMPASS-D and RF teams, Phys. Rev. Lett **85**, 574 (2000)

[Wilson 1996] H.R. Wilson, M. Alexander, J.W. Connor et al, Plasma Phys. Control. Fusion **38**, A149 (1996).

[Zhu 2006] W. Zhu, S. A. Sabbagh, R. E. Bell, J. M. Bialek, M. G. Bell, B. P. LeBlanc, S. M. Kaye, F. M. Levinton, J. E. Menard, K. C. Shaing, A. C. Sontag, and H. Yuh, Phys. Rev. Lett **96**, 225002 (2006).

[Zohm 1997] H. Zohm, D. A. Gates, H. R. Wilson, G. Gantenbein, O. Gruber, S. G. Gunter, M. Maraschek, A. W. Morris, M. Sokoll, D. Wagner, ASDEX Upgrade Team and COMPASS-D Team, Plasma Phys. Control Fusion **39** B237 (1997)